43

Tellus (1995), 47A, 697–704
Printed in Belgium – all rights reserved

TELLUS
ISSN 0280-6495

A life-cycle of nonlinear baroclinic waves represented by a simple 3-D spectral model

By H. L. TANAKA, *Institute of Geoscience, University of Tsukuba, Tsukuba 305, Japan*

(Manuscript received 29 August 1994; in final form 17 March 1995)

ABSTRACT

In this study, a life-cycle experiment for baroclinic disturbances is carried out for Simmons and Hoskins' 45° jet by integrating a three-dimensional spectral primitive equation model. The utility of the spectral representation in the vertical direction is examined for a fully nonlinear well-established phenomenon. The energy evolution and corresponding energy transformation are analyzed in the framework of the baroclinic-barotropic decomposition of atmospheric energy. According to the result, the initial perturbations of $n = 6$ grow exponentially drawing zonal baroclinic energy. This early evolution is reasonably described by linear baroclinic instability of the 45° jet. Both of baroclinic energy and barotropic energy of $n = 6$ increase simultaneously since the unstable mode maintains its consistent structure to grow. The energy flow is characterized as from zonal baroclinic energy via eddy baroclinic energy to eddy barotropic energy. These energy transformations are also synchronized since they are proportional to the eddy energy levels in the linear framework. When the waves reach the finite amplitude, the barotropic conversion increases, tranferring eddy barotropic energy toward zonal barotropic energy. It is shown by the result that the zonal barotropic energy increases when the waves decay, and the zonal jet is accelerated so that the structure becomes more barotropic. It is found by this study that the important baroclinic-barotropic interactions are coupled with baroclinic instability rather than the barotropic conversion. The results are consistent with previous studies. Therefore, we confirm also that the vertical spectral representation is applicable to simulate the nonlinear phenomenon.

1. Introduction

A numerical simulation of a life-cycle of nonlinear baroclinic waves was first conducted by Simmons and Hoskins (1978). According to their simulation, an initial perturbation superimposed on a zonal field grows exponentially by means of the baroclinic conversion, drawing zonal available potential energy to the perturbations. The basic process controlling the eddy growth is baroclinic instability (Charney, 1947). The amplified baroclinic disturbances start to transfer the energy back to the zonal kinetic energy by means of the barotropic conversion. The nonlinear baroclinic disturbances appear to accelerate the zonal jet at the end of their life-cycle as an expense of the zonal available potential energy. The energy flow analyzed by the simulated eddy activities is consistent with the understanding of the energy flow in the observed general circulation (Lorenz, 1955; Oort, 1964; Saltzman, 1970; Kung, 1988).

There should be no contradiction between the relaxed meridional temperature gradient and the accelerated zonal jet with reference to the thermal wind relation. The acceleration of zonal wind is supposed to occur at the lower troposphere and deceleration at the tropopause level so that the vertical wind shear diminishes. The role of the baroclinic disturbances on the structure change in the zonal motion is presented in Fig. 1 demonstrated by Hoskins (1983). An initial zonal mean flow (Fig. 1a) is modified at day 15 (Fig. 1b) by a single life-cycle of the wavenumber 6 disturbances so that the structure of the jet becomes more barotropic. The isentropic surface at day 15 indicates a relaxed meridional gradient in the mid-

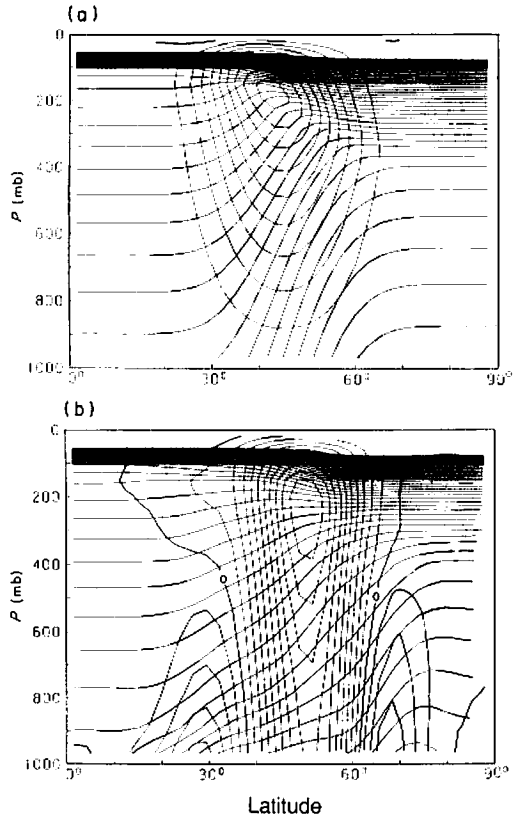

Fig. 1. Latitude-height cross sections showing potential temperature and zonal velocity in a baroclinic wave life-cycle experiment. Shown in (a) is the basic state and (b) the zonal field at day 15. The counter interval is 5 m/s for zonal velocity and 5 K for potential temperature (after Hoskins, 1983).

latitude, which implies a reduced zonal available potential energy. The core of the jet has moved north and the zonal kinetic energy has increased as will be confirmed later.

In this regard, more detailed analysis would be meaningful in order to understand the role of the baroclinic disturbances with a specific attention to the changes in the vertical structures of zonal and eddy fields.

In the present study, a life-cycle experiment is carried out for Simmons and Hoskins' 45° jet with initial perturbations of zonal wavenumber $n=6$ by integrating a 3-D spectral primitive equation model (Tanaka and Sun, 1990; Tanaka, 1991). Here, the vertical spectral expansion is applied for the discretization of governing primitive equations. The spectral model in the vertical direction is straightforward for the analysis of the energy redistribution in the vertical spectral domain. We use a set of vertical normal mode functions (Kasahara, 1984) for the construction of the vertical spectral model and analyze the energy transfer within the vertical spectral domain associated with the life-cycle of the baroclinic disturbances. The energy evolution and corresponding energy transformations are presented in the framework of a baroclinic-barotropic decomposition of atmospheric energy.

2. Model description

The governing spectral primitive equations are described in detail by Tanaka and Kung (1989) and Tanaka and Sun (1990). Thus a brief description of the model is given here. A system of primitive equations with a spherical coordinate of longitude λ, latitude θ, normalized pressure $\sigma = p/p_b$, and normalized time $\tau = 2\Omega t$ may be reduced to three prognostic equations of horizontal motions and thermodynamics. The three dependent variables are horizontal wind speeds, $V=(u, v)$, and geopotential deviation ϕ from the reference state of the global mean. Here, p_b and Ω are bottom pressure of the reference state and the angular speed of Earth's rotation, respectively. Using a matrix notation, these equations may be written as:

$$M\frac{\partial}{\partial\tau}U+LU=N+F, \tag{1}$$

where

$$U=(u, v, \phi)^{\mathrm{T}}. \tag{2}$$

The symbols M and L designate linear matrix differential operators with respect to the vertical and horizontal domains, N the nonlinear advection terms, and F the diabatic processes including frictional forces.

A 3-D spectral representation of the primitive equations can be derived by taking an inner product of (1) and basis functions of the 3-D normal mode functions $\Pi_{nlm}(\lambda, \theta, \sigma)$:

$$\left\langle M\frac{\partial}{\partial\tau}U+LU-N-F,\ Y_m^{-1}\Pi_{nlm}\right\rangle=0, \tag{3}$$

where

$$\Pi_{nlm}(\lambda, \theta, \sigma) = H_{nlm}(\lambda, \theta)\, G_m(\sigma), \tag{4}$$

$$Y_m = 2\Omega\, \mathrm{diag}(\sqrt{gh_m}, \sqrt{gh_m}, 1), \tag{5}$$

and the inner product is defined as

$$\frac{1}{2\pi}\int_{-\pi/2}^{\pi/2}\int_0^{2\pi}\int_0^1 \Pi^*_{nlm} \cdot \Pi_{n'l'm'} \cos\theta \, \mathrm{d}\sigma \, \mathrm{d}\lambda \, \mathrm{d}\theta$$

$$= \langle \Pi_{nlm}, \Pi_{n'l'm'} \rangle = \delta_{nn'}\, \delta_{ll'}\, \delta_{mm'}. \tag{6}$$

Here, $H_{nlm}(\lambda, \theta)$ and $G_m(\sigma)$ are Hough harmonics and vertical structure functions for zonal wavenumber n, meridional index l, and vertical index m, respectively. These three indices will be reduced to a single index i for short. The scaling matrix Y_m is defined with Earth's gravity g, and equivalent height h_m, for every vertical index. Refer to Tanaka and Sun (1990) for the detail of the definitions and the derivation. The vertical structure functions for the vertical indices $m = 0$ to 6 are illustrated in the Fig. 1 of Tanaka and Kung (1989). The vertical index $m = 0$ designates barotropic mode which has no mode in the vertical. The rest of the mth vertical modes have m nodes in the vertical showing a wavy structure with large amplitude at the top due to the effect of the density stratification. Those are referred to as baroclinic modes.

The resulting spectral primitive equations become a system of ordinary differential equations for Fourier expansion coefficients of variables:

$$\frac{\mathrm{d}w_i}{\mathrm{d}\tau} + i\sigma_i w_i = -i \sum_{j=1}^{M}\sum_{k=1}^{M} r_{ijk} w_j w_k + f_i,$$

$$i = 1, 2, \ldots, M, \tag{7}$$

where w_i and f_i are the expansion coefficients of the dependent variables and diabatic processes, σ_i are Laplace's tidal frequencies, r_{ijk} are interaction coefficients, and M is the total number of the series expansion for the 3-D atmospheric variables.

In this study, we consider diffusion, DF, as a single physical process. The scale dependency of diffusion is parameterized using the 3-D scale index σ_i based on the wave dispersion relating the wave scale and wave frequency. We approximate biharmonic-type diffusion for the Rossby (rotational) wave dispersion (for wavenumber $n \neq 0$) by:

$$(DF)_i = -K\left(\frac{n}{\sigma_i}\right)^2 w_i, \tag{8}$$

where K is a diffusion coefficient. Haurwitz waves on a sphere have phase speeds represented by the total wavenumber of the spherical surface harmonics $\hat{l}$ (see Swarztrauber and Kasahara, 1985):

$$c = \frac{-1}{\hat{l}(\hat{l}+1)} \simeq \frac{\sigma_i}{n}. \tag{9}$$

Since the diffusion is often approximated with $\hat{l}(\hat{l}+1)$, the present form of diffusion in (8) tends to be the biharmonic-type diffusion for higher order Rossby modes. For the zonal component, the meridional index l_R is substituted for $\hat{l}$.

The system of the nonlinear equations (7) is truncated to include only the Rossby modes for $m = 0$–6, $n = 0$ and 6, and $l_R = 0$–19. Note that the truncation is imposed in the frequency domain as well as in the wavenumber domain by excluding high-frequency gravity modes.

The initial condition is a northern zonal field of the 45° jet which is assumed to be symmetric about the equator. The most unstable linear mode is obtained by solving a matrix eigenvalue problem of the primitive equations linearized for this zonal field. Then, a small amplitude unstable normal mode is superimposed on the initial zonal field. The time integration is based on a combination of leap-frog and a periodic use of Euler-backward scheme. By virtue of the closure with the low-frequency subspace of the atmospheric modes, our model requires no implicit scheme and no artificial smoothing.

3. Results of the simulation

3.1. Structure

The model equation (7) is integrated in time with respect to the initial condition discussed above. The meridional height cross sections of geopotential amplitude for zonal wavenumber 6 are illustrated in Fig. 2. At day 2 in Fig. 2a, the maximum of the geopotential amplitude is seen at the mid troposphere over 50° N. The arrows in the figures describe the EP flux associated with the

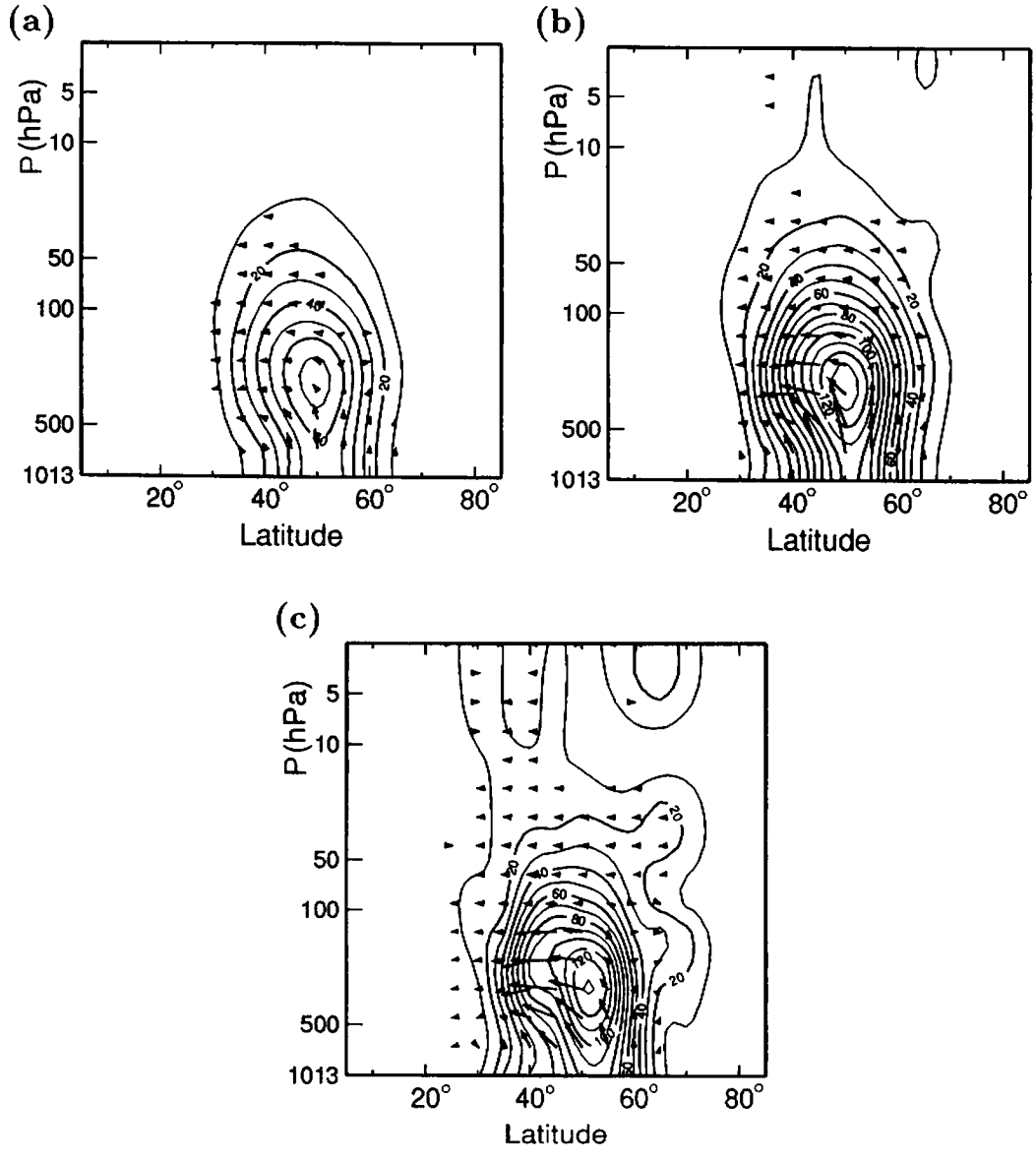

Fig. 2. Latitude-height cross sections of geopotential amplitude for wavenumber $n = 6$ and the associated EP flux during the life-cycle of the baroclinic wave. Shown in (a), (b), and (c) are for days 2, 4, and 6, respectively.

disturbances (e.g., Edmon et al., 1980; Hoskins, 1983). The EP flux is upward indicating large heat transport at the lower level. The structure is fundamentally the same as the most unstable linear mode (see Tanaka and Kung, 1989). At day 4 in Fig. 2b, the wave attains almost at its mature stage. The EP flux directs upward indicating acceleration of the zonal wind near the surface. The EP flux direction shifts for south at the upper troposphere decelerating the southern part of the zonal jet. At day 6 in Fig. 2c, the wave has passed its mature stage. The EP flux directs southward by this time showing dominant barotropic conversion.

The results shown here agree well with the

previous analysis by Hoskins (1983). The EP flux diverges near the surface and converges near the tropopause level, indicating the acceleration and deceleration of the zonal flow, respectively. As the result, the zonal jet becomes more barotropic as shown in Fig. 1.

3.2. *Energetics*

An element of total energy, E_i, for each basis function is defined in a dimensional form by

$$E_i = \tfrac{1}{2} p_b h_m |w_i|^2. \tag{10}$$

In order to explore the origin of the energy supply for the unstable baroclinic waves, an energy flow box diagram describing energy interactions between barotropic and baroclinic components is constructed. By differentiating (10) with respect to time and substituting (7), we obtain for eddy:

$$\frac{dE_i}{dt} = 2\Omega p_b h_m \Sigma_j \mathrm{Re}(ib_{ij}^* w_j^* w_i)_{m''=0} + 2\Omega p_b h_m \Sigma_j \mathrm{Re}(ib_{ij}^* w_j^* w_i)_{m''\neq 0} = C(B_{m''=0}, E_i) + C(B_{m''\neq 0}, E_i). \tag{11}$$

Note that the linear term in the left-hand side of (7) does not contribute to the energy balance equation. The first term of the right-hand side of (11) stands for energy transformations from the barotropic component of the zonal field $B_{m''=0}$ into E_i, and the second term represents those from the baroclinic components of the zonal field $B_{m''\neq 0}$ into E_i (refer to Tanaka and Kung, 1989). By adding all indices separately for $m=0$ and $m\neq 0$, (11) becomes:

$$\frac{dE_{m=0}}{dt} = C(B_{m''=0}, E_{m=0}) + C(B_{m''\neq 0}, E_{m=0}), \tag{12}$$

$$\frac{dE_{m\neq 0}}{dt} = C(B_{m''=0}, E_{m\neq 0}) + C(B_{m''\neq 0}, E_{m\neq 0}). \tag{13}$$

The resulting energy flow box-diagrams are presented in Fig. 3 for the most unstable Charney mode at $n=6$. Upper boxes ($m''\neq 0$, $m\neq 0$) denote the baroclinic components and lower boxes ($m''=0$, $m=0$) the barotropic components for $n=0$ and 6, respectively. In the figure the energy interactions in (12) and (13) are rearranged further so that the energy is transferred along the lines denoted in the energy flow box diagram based on the fact that there is no barotropic-baroclinic interaction for the zonal geostrophic (rotational) modes.

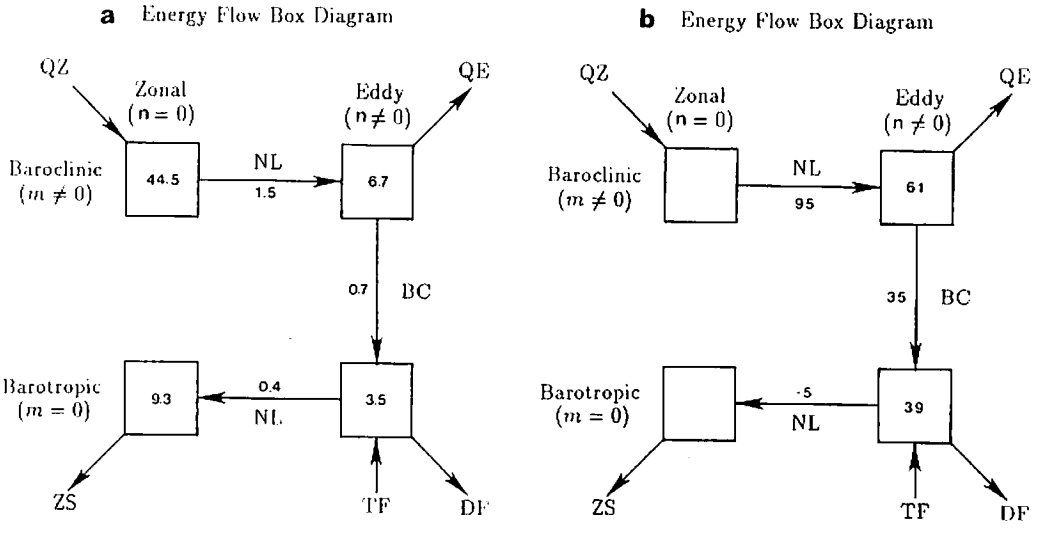

Fig. 3. Energy flow box diagram within zonal and eddy energies decomposed in barotropic and baroclinic components. (a) FGGE observation, (b) unstable Charney mode for $n=6$. Units are 10^5 J m^{-2} for energy and W m^{-2} for energy conversions. Percentile contributions are substituted for (b).

It is evident from the result that large proportions of energy are transformed from zonal baroclinic energy to eddy baroclinic energy then to eddy barotropic energy for the growing modes. The result evaluated with FGGE observations is also illustrated in Fig. 3 for comparison. The observed atmospheric energy flow clearly represents the characteristic of energy flow due to the baroclinically unstable modes.

3.3. *Evolution of barotropic and baroclinic energies*

Fig. 4 shows time evolutions of energy and energy conversions discussed in Fig. 3 for a life-cycle of the nonlinear baroclinic disturbances. As shown in Fig. 4, the initial perturbations of $n=6$ grow exponentially drawing zonal baroclinic energy. This early stage of the evolution is reasonably explained by linear baroclinic instability of the 45° jet. Both of baroclinic energy and barotropic energy of $n=6$ increase simultaneously because the unstable mode maintains its consistent structure to grow. The energy flow is characterized as from zonal baroclinic energy via eddy baroclinic energy to eddy barotropic energy. These energy transformations are also synchronized because they are proportional to the eddy energy levels in the linear framework.

When the waves reach the finite amplitude, the barotropic conversion increases, transferring the accumulated eddy barotropic energy toward zonal barotropic energy. Accordingly, zonal barotropic energy increases when the synoptic waves decay. It is shown that the zonal jet is accelerated so that the structure becomes more barotropic. The result presented in the framework of the barotropic-baroclinic decomposition is straightforward to describe this fact and is consistent with previous studies.

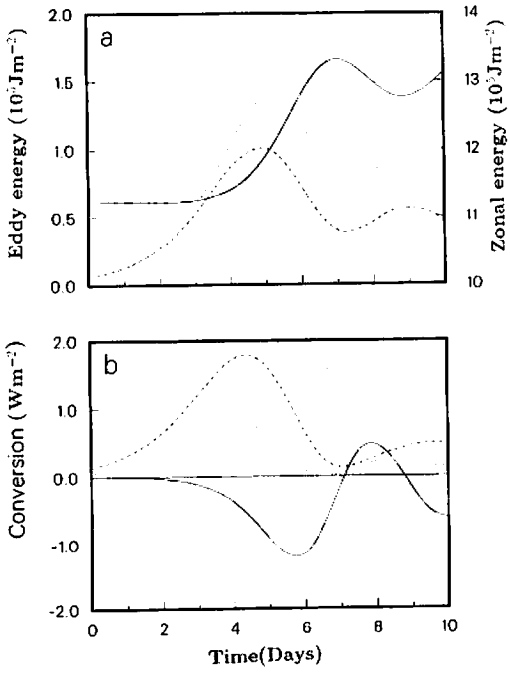

Fig. 4. (a) Time evolutions of eddy baroclinic energy (dashed line), eddy barotropic energy (dotted line), and zonal barotropic energy (solid line with its scale at right ordinate) for $n=6$. Units are 10^5 J m^{-2}. (b) Time evolutions of energy conversions from zonal baroclinic to eddy baroclinic energies (dashed line), from eddy baroclinic to eddy barotropic energies (dotted line), and from eddy barotropic to zonal barotropic energies (solid line). Units are W m^{-2}.

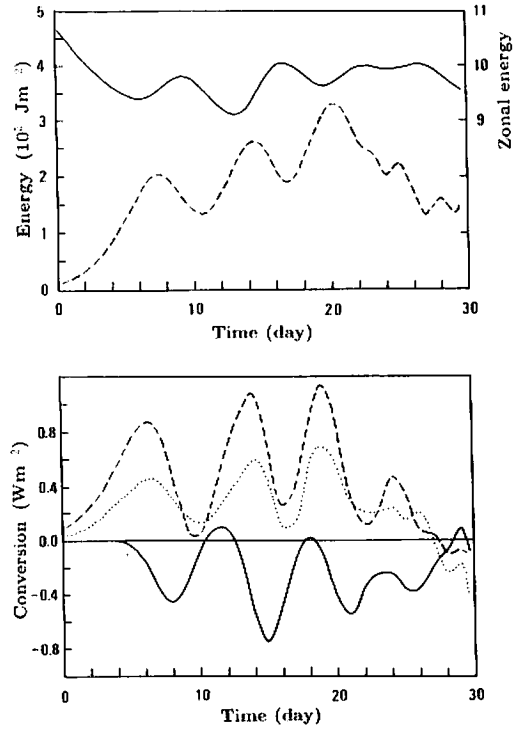

Fig. 5. Time evolutions of energy and energy conversions as in Fig. 4, but for an experiment with a restoring zonal baroclinic field. The eddy energy (dashed line) is the sum of the barotropic and baroclinic components.

The important process in baroclinic instability is the zonal-wave interaction due to the eddy heat flux and the simultaneous baroclinic conversion at each zonal wavenumber. This baroclinic conversion is fundamentally a linear process. In contrast, the upscale zonal-wave interaction of the barotropic conversion is essentially a nonlinear process. It is found from Fig. 4 that the important baroclinic-barotropic interactions are coupled with linear baroclinic instability rather than the nonlinear barotropic conversion.

Fig. 5 illustrates the time evolutions of energy and energy conversions as seen in Fig. 4. During this simulation, the largest meridional components of the zonal baroclinic field ($m = 4$) are treated as steady to maintain the meridional temperature gradient due to the differential heating. The diffusion coefficient is slightly increased in order to balance with the increased energy supply. As a result, we find that the baroclinic disturbances repeat the life-cycle for several times, drawing the energy from the zonal baroclinic components and feeding the zonal barotropic jet. The role of the baroclinic disturbances is therefore evident to pump the zonal energy from the baroclinic to the barotropic components.

4. Concluding remarks

A life-cycle of nonlinear baroclinic waves is examined in terms of the barotropic-baroclinic decomposition of zonal and eddy fields. The energy flow is characterized as from zonal baroclinic energy via eddy baroclinic energy to eddy barotropic energy. The barotropic conversion follows when the waves reach the finite amplitude, transferring the accumulated eddy barotropic energy toward zonal barotropic energy. As a result, zonal barotropic energy increases when the synoptic waves decay. It is found in this study that the important baroclinic-barotropic interactions occur along with (linear) baroclinic instability rather than the (nonlinear) barotropic conversion.

We can clearly observe the time lag (about 2 days) between the relaxation of the meridional temperature gradient and the acceleration of the zonal jet due to the life-cycle of the nonlinear baroclinic disturbances. The jet is accelerated so that the structure becomes more barotropic in the vertical. This means that the zonal wind is accelerated at the lower troposphere, where the frictional dissipation is most efficient in a real atmosphere.

It may be concluded by this study that the role of the nonlinear baroclinic disturbances is to convert the zonal energy supplied by the differential heating toward the barotropic component of motions so that the energy is most efficiently dissipated by the surface friction.

5. Acknowledgments

This research was jointly supported by the Sumitomo Foundation under the contract number 93-104-457 and by Grant-In-Aid from the Ministry of Education under the number 05NP0203 and 05452077. The author is grateful to K. Kimura and K. Itoh for their technical assistance.

REFERENCES

Charney, J. G. 1947. The dynamics of long waves in a baroclinic westerly current. *J. Meteor.* **4**, 135–162.

Edmon, H. J., Hoskins, B. J. and McIntyre, M. E. 1980. Eliassen-Palm cross-sections for the troposphere. *J. Atmos. Sci.* **37**, 2600–2616.

Hoskins, B. J. 1983. Modelling of the transient eddies and their feedback on the mean flow. *Large-scale dynamical processes in the atmosphere* (eds. B. J. Hoskins and P. P. Pearce). Academic Press, 169–199.

Kasahara, A. 1984. The linear response of a stratified global atmosphere to tropical thermal forcing. *J. Atmos. Sci.* **41**, 2217–2237.

Kung, E. C. 1988. Spectral energetics of the general circulation and time spectra of transient waves during the FGGE year. *J. Climate* **1**, 5–19.

Lorenz, E. N. 1955. Available potential energy and the maintenance of the general circulation. *Tellus* **7**, 157–167.

Oort, A. H. 1964. On the energetics of the mean and eddy circulations in the lower stratosphere. *Tellus* **16**, 309–327.

Saltzman, B. 1970. Large-scale atmospheric energetics in the wavenumber domain. *Rev. of Geophys. and Space Phys.* **8**, 289–302.

Simmons, A. J. and Hoskins, B. 1978. The life cycles of some nonlinear baroclinic waves. *J. Atmos. Sci.* **35**, 414–432.

Swarztrauber, P. N. and Kasahara, A. 1985. The vector harmonic analysis of Laplace's tidal equation. *SIAM J. Sci. Stat. Compute* **6**, 464–491.

Tanaka, H. L. 1991. A numerical simulation of amplification of low-frequency planetary waves and blocking formations by the upscale energy cascade. *Mon. Wea. Rev.* **119**, 2919–2935.

Tanaka, H. L. and Kung, E. C. 1989. A study of low-frequency unstable planetary waves in realistic zonal and zonally varying basic states. *Tellus* **41A**, 179–199.

Tanaka, H. L. and Sun, S. 1990. A study of baroclinic energy sources for large-scale atmospheric normal modes. *J. Atmos. Sci.* **47**, 2674–2695.